electronics

MDPI

Article

Dimming Techniques Focusing on the Improvement in Luminous Efficiency for High-Brightness LEDs †

Kun-Che Ho [1], Shun-Chung Wang [2,*] and Yi-Hua Liu [1]

[1] Department of Electrical Engineering, National Taiwan University of Science and Technology (NTUST), Taipei 106335, Taiwan; D10507001@mail.ntust.edu.tw (K.-C.H.); yhliu@mail.ntust.edu.tw (Y.-H.L.)
[2] Department of Marine Engineering, National Taiwan Ocean University (NTOU), Keelung City 202301, Taiwan
* Correspondence: shunchung.wang@gmail.com; Tel.: +886-2-910-334-575

† This paper is a rewritten and extended article recommended to *Electronics* after presented at the 4th IEEE International Conference on Knowledge Innovation and Invention 2021 (ICKII 2021) on 23–25 July 2021 in Taichung, Taiwan. (Paper No.: K210046).

Abstract: The pulse width modulation (PWM) dimming mode features good dimming linearity and has been widely used for driving high-brightness light-emitting diodes (HBLEDs), in which the brightness change is reached by modulating the duty cycle of the dimming signal to regulate the average current flowing through LEDs. However, the current-illuminance characteristic curve of most LEDs is nonlinear in nature. Namely, under the same lighting power fed, the conventional PWM dimming cannot make the LED exert its best luminous efficiency (LE) specified in datasheets. This paper focuses on the study of further improving LED luminous efficacy via dimming manipulation. Thereby, two multilevel current dimming techniques with varied dimming signal voltage and varied current sensing resistance are presented. With limited dimming capability, the proposed dimming strategies can efficiently raise the luminous flux ratio without increasing the power consumption. A prototype constructed for a 115 W HBLED driver is developed and the devised dimming schemes are realized by a digital signal controller (DSC). Experimental results exhibited with illuminance-power curves and CIE1931 and CIE1976 chromaticity diagrams are given to validate the theoretical derivation and effectiveness. Compared with conventional PWM dimming, under the same illuminance, the driver average output power is respectively reduced by 17.08% and 13.17%; the improvement in average illuminance under the same output power is 13.66% and 11.17%, respectively. In addition, the entire average LE boost has respectively increased by 21.36% and 16.37%.

Keywords: dimming control; high-brightness light-emitting diode (HBLED); luminous efficiency

Citation: Ho, K.-C.; Wang, S.-C.; Liu, Y.-H. Dimming Techniques Focusing on the Improvement in Luminous Efficiency for High-Brightness LEDs. *Electronics* **2021**, *10*, 2163. https://doi.org/10.3390/electronics10172163

Academic Editor: Marco Mussetta

Received: 7 August 2021
Accepted: 2 September 2021
Published: 4 September 2021

1. Introduction

In recent years, solid-state lighting (SSL) components have become the mainstream light source in many lighting applications. Most emerging SSL varieties, compared with conventional illuminant sources, have the great advantages of energy saving, a long life span, chromatic variety, less heat generation, fast response, and an ecofriendly nature [1–10]. With remarkable advances in manufacturing processes and in material technology, the luminous efficiency of light-emitting diodes (LEDs) has been significantly boosted and the cost has become more accessible to people [11–15]. This makes LED applications more and more diversified and the traditional lighting fixtures used in street lamps, screen displays, indoor and outdoor lighting, etc., are gradually being replaced by LED ones. According to a report updated by the Department of Energy, U.S., at the end of 2019, LEDs accounted for about 37% of the lighting equipment in the U.S. area and roads in 2017. It is estimated that by 2025 and 2035, the installation rate of LED-based lighting fixtures will reach 92% and 98%, respectively [16]. The luminous characteristics of LEDs is directly related to its through forward current, but the relationship between the forward current and the voltage drop of the LED is nonlinear and is related to the operating temperature. A

small forward voltage variation may result in a very dramatic increase in forward current. Accordingly, the LED is unsuitable for driving directly with a constant voltage source, yet most LED drivers have been designed to dim the illumination by the precise control of a forward current to specified values. In addition, for driving multiple LED strings in parallel, in order to achieve uniform brightness, a current equalization mechanism is also indispensable [17–21].

An efficient LED driver with an effective dimming control is essential to curtail energy consumption, color spectrum shift, and to adjust luminous intensity via the exact current modulation. A dimmable LED fixture consists of a driver, several LED strings, and a dimmer. The driver receives a dimming signal from the dimmer based on the dimming rule realized to regulate the forward current in response to the dimming manipulation. Different dimming techniques or functions employed will bring diverse concerns to their impact on a visible light flickering to a human eye and the power quality of a grid [20–22]. Therefore, a large number of new driver topologies have been proposed to raise the driver efficiency and power density [23–27]. On the other hand, many literatures focus on the research of novel dimming and current control methods that can achieve more luminosity flux generation with the least energy consumption to further meliorate the entire driving performance. In general, among the currently proposed LED driving and dimming methods driving an LED with a dc source, the luminosity output surpasses all the other techniques. However, the PWM driving mode offers a greater dimming flexibility and linearity in comparison with the dc manner, as the dimmable function is the first consideration priority. In Ref. [28], for improving dimming efficiency, a synchronous integration method was presented to make the output voltage self-adaptable. Besides, to solve the poor linearity of the dimming curve when dimming at a low illuminance, the variable dimming frequency is adopted to replace a fixed frequency one. In Ref. [29], a multilevel PWM dimming method (MPWM) was studied to tackle the problem of a low luminous efficiency that occurs in conventional PWM dimming. The MPWM driving can achieve a higher luminous efficacy compared to the conventional PWM way, while maintaining the characteristic of duty-cycle-based dimming. A single-inductor multi-floating output circuit was adopted in [30] to cope with the low dimming frequency and energy loss problems arising from the single-inductor multi-output circuit, and an average current correction technique was proposed to deal with the current imbalance and dimming efficacy caused by the different forward voltage drop of each LED string. An analysis model including the luminous flux, correlated color temperature (CCT), electrical power, and junction temperature of the white LED sources with a bi-level driver is studied in Ref. [31] The proposed method can improve the luminous flux variation and color shift of the LED. Diminution in variation of luminous flux and CCT over a dimming range has been accomplished also. In Ref. [32], an improved bi-level LED driving approach is put forward. It includes high/low PWM current levels and duty cycles to provide a 2-D luminosity control capability and to reduce the energy consumption. This proposed method can also be derived to an n-level driving way for bettering the electrical-to-light conversion efficiency of LEDs. A general n-level driving approach based on the PWM driving mode is proposed in Ref. [33] to improve the luminous efficacy of lighting devices, which have the fast and saturable electrical-to-optical conversion characteristic while maintaining the primary control flexibility of the usual PWM-mode driving. The proposed method uses multiple power supplies with different output voltages to supply different currents to drive LEDs. This makes the brightness curve of PWM dimming closer to the amplitude-mode dimming technique. Literature [34] put forth a general method, which features the characteristics of PWM dimming and dc dimming. A pulsating current, switched between two separate levels, with adjustable levels and their durations at the same time, is supplied to map the driving conditions to the light output more accurately.

On the other hand, the relationship between the generated light flux and the fed current of most LEDs is not linear in nature. Take the CREE CXB1304 LED array [35] as an example; the curve of current versus relative luminous flux ratio (RLFR) under 25 °C is illustrated in Figure 1. From Figure 1, it can be found that the output luminous

flux intensity is very sensitive to current variations. The smaller the forward current flowing through, the greater the ratio of illuminance to the current, and it will gradually degrade as the operation current increases. For commonly used digital PWM dimming, the brightness change is achieved by modulating the duty cycle of the dimming signal to regulate the average current flowing through LEDs, i.e., the current through the LED is alternate between zero and the rated value, rather than changing the amplitude of its forward current. It can be also seen from Figure 1 that when the LED current is 500 mA, the corresponding RLFR is about 230%, but if the average current is regulated to 250 mA controlled by PWM dimming, only 115% RLFR can be attained, rather than the 135% one obtained from the original characteristic curve. As a result, due to the nonlinearity of current versus illuminance behavior, the same power fed to light the LED with PWM dimming cannot emit the brightness that it should have. In other words, it cannot achieve the best luminous efficiency conversion specified in its specifications. Accordingly, in this study, to focus on further improving the electricity-to-light conversion efficacy of LEDs, two multilevel current dimming methods respectively with varied dimming signal voltage (VDSV) and varied current sensing resistance (VCSR) are presented. The main contributions of this paper are that, with limited dimming capability, the proposed dimming strategies can effectively boost the luminous efficacy without needing more power consumption as compared with the PWM dimming mode. Besides, the proposed LED driver is constructed by uncomplicated and reliable converters based on the manipulation of a low-cost DSC with minimum computational effort. The rest of the paper is organized as follows. Section 2 introduces the system architecture and design consideration of the developed LED driver. The operating principle and manipulation of the proposed dimming controls are derived in Section 3. In Section 4, the measured experimental results are exhibited to verify the prototype constructed, and then comparisons with the conventional counterpart are made to demonstrate the effectiveness and performance improvement of the proposed dimming scheme. Finally, Section 5 concludes this paper.

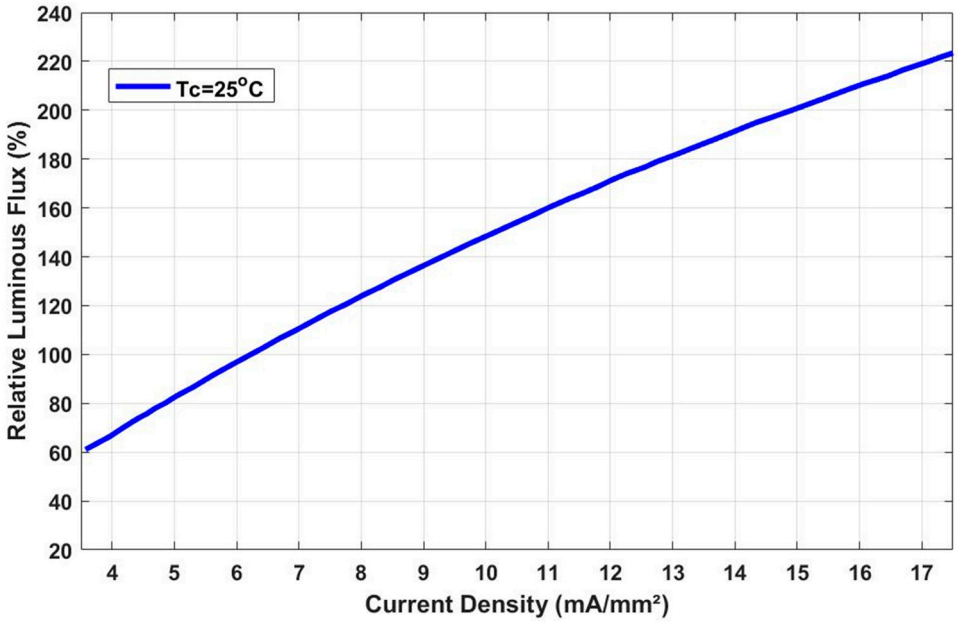

Figure 1. Curve of current density vs. RLFR for CXB1304 LED array under 25 °C.

2. Configuration of the Studied LED Driver

Figure 2 shows the architecture of the LED driver with a high luminous efficiency as studied in this paper. This driver is composed of a voltage-mode-controlled buck converter to feed LED power, a current control circuit with current sensors to balance LED currents, a dimming manipulator with a buck controller and devised dimming approaches realized by firmware and written into a digital signal controller (DSC) dsPIC33FJ16GS502 from

Microchip to regulate LED voltage and fulfil dimming functions, as well as dimmable white HBLED modules connected in one series and ten parallel (1S10P) patterns to serve as a light source. The buck output voltage V_o is sampled (the ADC_V) with a 35 kHz sampling frequency and then digitized by an analog-to-digital converter (ADC) inside the DSC. The noises of quantized value are filtered by the developed 32-order digital finite impulse response (FIR_v) filter and is sent to the PID_{SW} compensator (with gains of K_p = 0.028, K_i = 44.92, $K_d = 4.49 \times 10^{-6}$) to calculate the duty cycle required. The target duty cycle is routed to the PWM module (PWM_{SW}) for generating the gating control signal (PWM_{GD}) of SW to regulate the V_o.

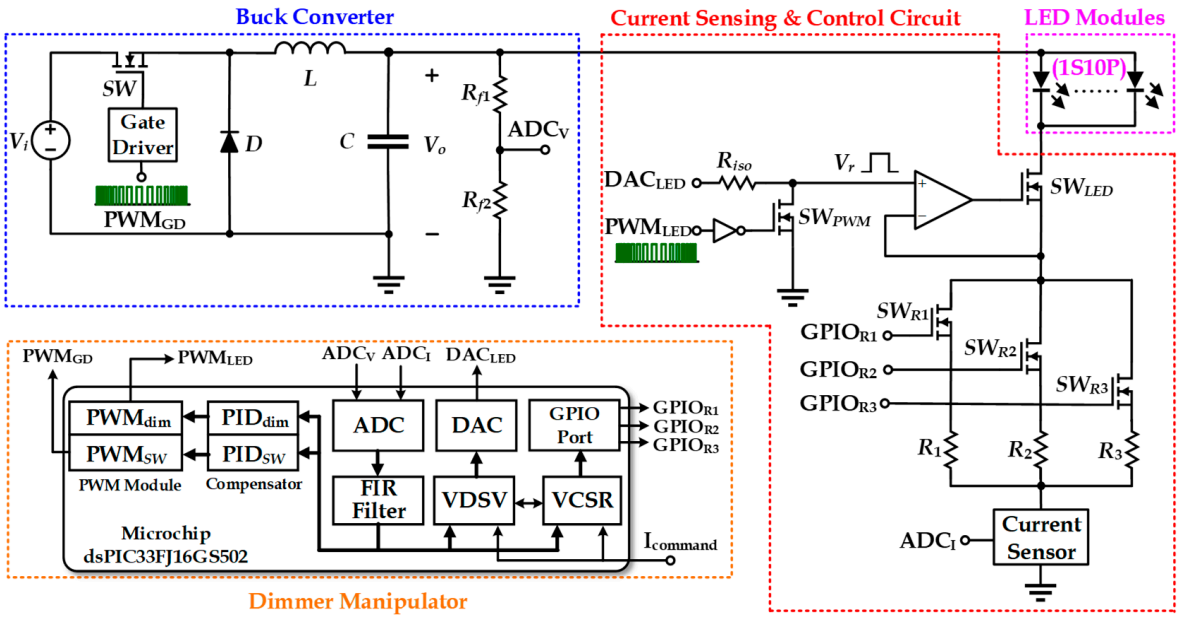

Figure 2. Configuration of the LED driver studied.

Similarly, to accurately control the LED current, the current flow through LEDs must be sampled (the ADC_I), digitized, and filtered by the current sensor, ADC with a 300 Hz sampling frequency, and the 32-order FIR_I filter. For the proposed two VDSV and VCSR dimming methods, the quantized feedback current value (the FIR_I output) is compared with the dimming command ($I_{command}$). According to the current error, the VCSR method computes the required total sensing resistance value that can generate the LED current as the command specified, and then outputs the gating control signal ($GPIO_{R1}$~$GPIO_{R3}$) by the general purpose I/O (GPIO) port to switch SW_{R1}~SW_{R3} to obtain the resistor parallel pattern and the dimming current of each level required. On the other hand, based on the digital error values, the VDSV method will figure out the required level (amplitude) of the dimming signal V_r that can generate the LED current as a command set. Thereby, the corresponding analog voltage level (DAC_{LED}) can output after conversion by the DAC, and then cooperates with the gating control signal (PWM_{LED}) generated by the dimming PWM module (PWM_{dim}) to switch SW_{PWM} to obtain the desired V_r and the target dimming current of each level. Where 300 Hz dimming frequency is selected here and the target LED average current for luminosity control can be obtained by modulating the duty cycle of the dimming signal that is derived from the calculation of a PID_{dim} compensator (with gains of K_p = 5.026, K_i = 25.13, $K_d = 2.51 \times 10^{-11}$) in advance. The following will introduce the main parts of the LED driver, and the proposed dimming methods will be described in detail in a later section.

2.1. Buck Converter and Design Consideration

The buck converter, as illustrated in Figure 2, is served as the power stage of the LED drive. It operates in a continuous conduction mode (CCM). The L and C constitute a two-pole low-pass filter to filter high-frequency switching harmonics to meet the ripple specification. The output voltage V_o needed to power LED strings can be regulated by modulating the duty cycle of the power switch (SW). Figure 3 shows the inductor voltage (v_L) and current (i_L) waveforms of a buck converter in CCM operation. In steady state, based on the volt-second balance of the inductor, the net change of the flux linkage within a switching period T_s is zero, and this make the average voltage across the inductor zero too. Hence, the voltage conversion ratio $M(D_{on})$ of a buck converter in CCM can be derived as follows:

$$(V_i - V_o)D_{on} - V_o(1 - D_{on}) = 0 \Rightarrow M(D_{on}) \equiv \frac{V_o}{V_i} = D_{on} \tag{1}$$

where V_i and V_o stand for input and output voltages and D_{on} is the duty cycle of the SW. The peak-to-peak change in the inductor current Δi_L is equal to the i_L slope times the length of the first switching subinterval, so the desired inductance value can be derived by

$$\Delta i_L = \frac{V_i - V_o}{L} D_{on} T_s \Rightarrow L = \frac{V_i - V_o}{\Delta i_L} D_{on} T_s \tag{2}$$

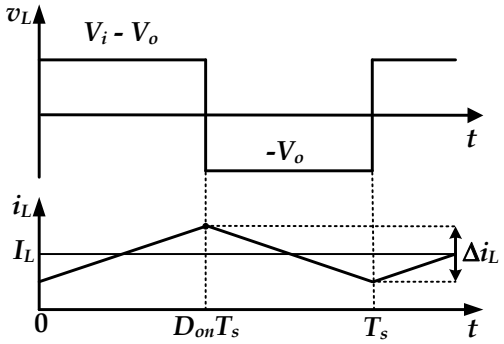

Figure 3. Waveforms of inductor voltage (v_L) and current (i_L) in CCM.

The charge change (Δq) in the output filter capacitor (C) is related to the capacitance value and the peak-to-peak output voltage ripple ΔV_o, which can be expressed as $\Delta q = C \cdot (\Delta V_o)$. That is, the incremental charge is the integral of the i_L waveform between its zero crossings. For the buck converter, it can be denoted by

$$\Delta q = \frac{T_s \Delta i_L}{8} = C\Delta V_o \Rightarrow \Delta V_o = \frac{T_s \Delta i_L}{8C} \tag{3}$$

If the output voltage ripple is specified, the required filter capacitor value C which met the ripple specification can be calculated using (3). Substituting (1) and (2) into (3), the C can be obtained by

$$C = \frac{V_o(1 - D_{on})T_s^2}{8L\Delta V_o} \tag{4}$$

According to the LED rating specified in the datasheet [35], when the temperature is 25 °C and the current is 500 mA, the forward voltage drop is about 19.5 V. Besides, based on the LED connection pattern (1S10P) in this study, and coupled with the voltage drops across the current sensing resistor and the drain-source of the SW_{LED}, the nominal output voltage (V_o) and current (I_o) are designed to 23 V and 5 A respectively. The percentage peak-to-peak output voltage and inductor current ripples are specified at ±2% and ±20%, respectively. Accordingly, the rated output power (P_o) is 115 W. The nominal input voltage (V_i) is set to 84 V if a step-down power factor correction pre-regulator is equipped. In addition, in consideration of the power semiconductor component selection, when the

MOSFET and diode are off or on, the blocking voltage or carrying current must be greater than the maximum values of the input or output voltage or current, respectively. Table 1 summarizes the design specifications of the buck converter and the current control circuit studied, as well as the part numbers and ratings of the adopted components. In addition, parasitic or stray parameters often exist in the circuit implementation. These parameters are mainly derived from the non-ideal characteristics of the power semiconductor components (*SW* and *D*) used and the layout wires on the PCB board under high-frequency operation. Since the output and junction parasitic capacitances of the switching elements selected is very small, it has very little influence on the results obtained. Besides, the selected switching frequency (f_s) is 35 kHz. In general, stray inductance will only reveal its effect at high frequency, so in the realized circuit, the effect of stray inductance on the measured results is also very insignificant. On the other hand, there are some stray sources in the circuit and non-ideal characteristics of the components, which will cause nonlinear phenomena to the system function. Nevertheless, from Equation (1), the relationship between the buck output and the input voltages is linear in the CCM operation mode. Furthermore, via the effective feedback control loop designed, the impact of these nonlinear effects on the measured results still can be properly controlled within an acceptable range.

Table 1. Design specifications and selected parameter values of components of buck converter and current control circuit.

Buck Converter			
Item	**Design Spec.**	**Item**	**Part No. and Rating**
V_i	84 V	L	1 mH
V_o	23 V	C	100 µF
I_o	5 A	D	STPS20150C (150 V/20 A)
P_o	115 W	SW	IPP030N10N3G (100 V/100 A)
f_s (=1/T_s)	35 kHz	-	-
Current Control Circuit			
Item	**Part No. and Rating**	**Item**	**Part No. and Rating**
OPA	LM324	SW_{LED}	IPP200N25N3 (250 V/64 A)
$SW_{R1,2.3}$	IPP200N25N3 (250 V/64 A)	SW_{PWM}	2N7002 (60 V/0.3 A)

2.2. Linear Current Control Circuit

Driving LEDs have a constant current, which not only allows the LED to reach a stable current, but also improves the forward current fluctuation caused by the LED internal resistance change because of the temperature rise. Figure 4a shows the scheme of the linear current control (LCC) circuit. It consists of an operational amplifier (OPA), a resistor R_S for a sensing pass current and a power switch SW_{LED} operated in the linear region. The V_r is a dimming control that is signal fed. When the OPA output V_G is at a high level, the SW_{LED} gets in the conduction state, and it is equivalent to a variable resistor. The current I_o is fed back to the OPA through the R_S for comparison with V_r. When the V_r is low, the SW_{LED} will be turned off. In addition, from the feedback control system of the LCC circuit, it can be observed that the LCC system is voltage input and current feedback, so this is a series–series feedback amplifier. Figure 4b plots its open loop equivalent circuit model. Where, r_i, r_{o1}, A_{OL}, and V_d are the input impedance, output impedance, open loop gain, and voltage difference between non-inverting and inverting input terminals of the OPA, respectively. g_m and r_{o2} are the transconductance and the equivalent resistance across drain and source of the MOSFET (SW_{LED}), respectively. Vs is the current sensing feedback signal. V_o and I_o' are the output voltage and currents of the driver. R_{LED} is the LED on resistance. From Figure 4b, if r_{o1} is neglected, the following relevant circuit parameters can be first derived as follows:

$$\beta = \frac{V_S}{I_o} = R_S \tag{5}$$

$$V_G = A_{OL} \cdot V_r' \cdot \frac{r_i}{r_i + R_S},\ V_S = I_o' \cdot R_S,\ V_D = -I_o' \cdot R_{LED} \tag{6}$$

$$I_o' = g_m \cdot V_{gs} + \frac{V_{DS}}{r_{o2}} = (V_G - V_S) \cdot g_m + \frac{V_D - V_S}{r_{o2}} \tag{7}$$

where β is feedback gain. V_G and V_D are the gate and drain voltages of SW_{LED}. Substituting (5) and (6) into (7), the system open loop gain A can be calculated as

$$A = \frac{I_o'}{V_r'} = \frac{A_{OL} \cdot g_m \cdot \frac{r_i}{r_i + R_S}}{1 + R_S \cdot g_m + \frac{R_{LED} + R_S}{r_{o2}}} \tag{8}$$

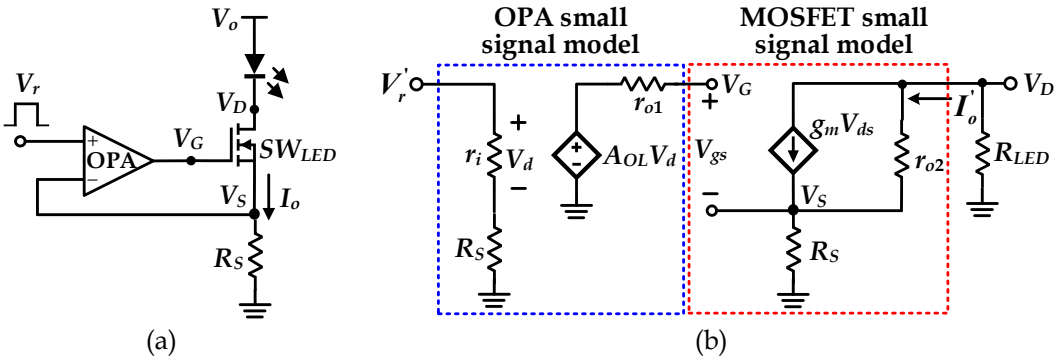

Figure 4. Linear current control circuit: (**a**) Basic topology; (**b**) Equivalent circuit model of (**a**).

Assuming that $r_i >> R_S$ and r_{o2} is close to infinity, then (8) can be simplified by

$$A = \frac{I_o'}{V_r'} = \frac{A_{OL} \cdot g_m}{1 + R_S \cdot g_m} \tag{9}$$

Therefore, the closed loop gain A_f of the LCC circuit can be figured out as

$$A_f = \frac{I_o}{V_r} = \frac{A}{1 + A\beta} = \frac{A_{OL} \cdot g_m}{1 + R_S \cdot g_m + A_{OL} \cdot g_m \cdot R_S} \tag{10}$$

Due to the $A_{OL} \cdot g_m \cdot R_S >> 1 + g_m \cdot R_S$, thus (10) can be simplified as

$$A_f = \frac{I_o}{V_r} \simeq \frac{1}{R_S} \simeq \frac{1}{\beta} \tag{11}$$

3. Proposed Dimming Control Method

It can be known from the derivation of above subsection that the LED forward current can be regulated by changing the voltage level of V_r or the resistor value of R_S. Under the same power fed to light LEDs, the PWM dimming mode cannot make the LED generate the illuminance that it should have originally as written down in its specifications. Hence, this paper is specifically aimed at further bettering the luminous efficiency of LEDs, and thus two multilevel current dimming mechanisms with varied current sensing resistance (VCSR) and varied dimming signal voltage (VDSV) are studied. The following subsections will expound the operating principles and implementation processes of the two proposed methods.

3.1. The Dimming with VCSR

According to the current–illuminance curve illustrated in Figure 1, the illuminance of the CXB1304 LED was measured actually by changing the value of the current sensing resistor (R_S) to dim the LED. In this method, the dimming signal V_r is fixed to a preset value. Figure 5 shows the current–illuminance curves measured under different R_S values.

It can be seen from Figure 5 that, as the illuminance value is the same, the larger the R_S value, the smaller the driver output current. On the other hand, as the fed forward current is identical, the larger the R_S value is, the larger the LED illumination that will be obtained. Therefore, when more R_S with different resistance values are used for dimming control, the power saving effect will be more obvious, and thus the luminous efficiency will be better. The derivation of determining the number and value of R_S needed to carry out the multilevel current dimming is described as follows.

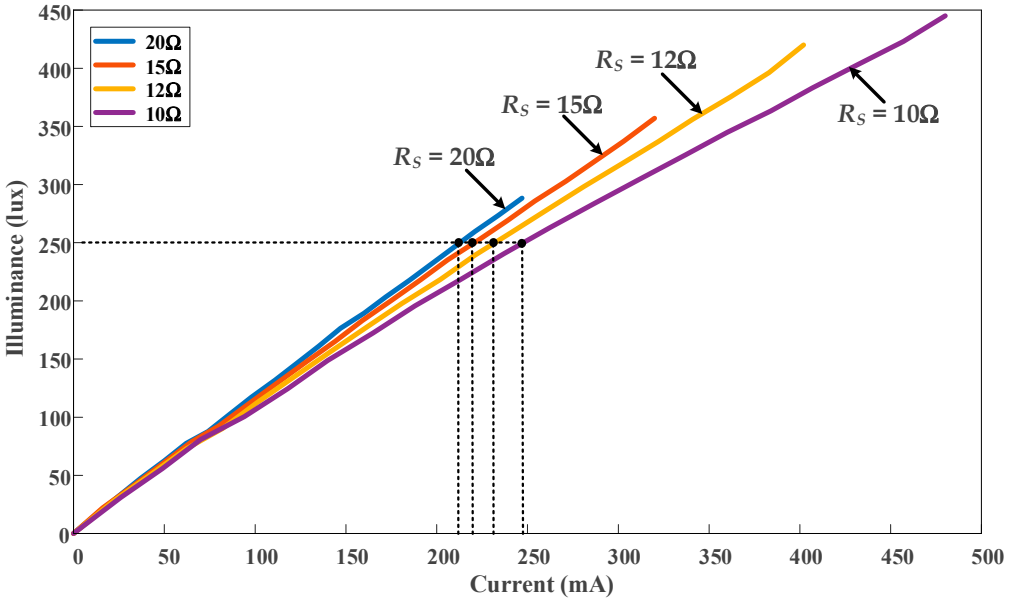

Figure 5. Measured current–illuminance curves for CXB1304 LED under different R_S values.

Figure 6 shows LED illumination characteristics of the original and those obtained by the other three PWM controls with different current levels. To simplify the derivation process and control complexity, a three-level current dimming control is taken as an example here. As depicted in Figure 6, because the linear PWM dimming control is adopted, to exert the best LED electricity-to-light conversion efficiency, it is necessary to find the suitable transition value of the dimming control current in each level. Furthermore, in order to be controllable in the full current range operated, one level must be set to the LED rated current, i.e., the I_7, yet the remaining two-level currents, i.e., the I_4 and I_6, must be found. In Figure 6, PWM1, PWM2, and PWM3 respectively represent the illuminance curves obtained by different levels of PWM dimming control, and I_4, I_6 and I_7 stand for the maximum acceptable current transition value of each level that it can offer to the sensing resistance value used. The three areas enclosed by the gray regions are calculated using integration, i.e., the illuminance area enclosed by PWM1 dimming is integrated from 0 to I_4; the illuminance area enclosed by PWM2 dimming is integrated from I_4 to I_6; and the illuminance area enclosed by PWM3 dimming is integrated from I_6 to I_7. The area figured out is a function of the dimming current at each level. The total area enclosed by the three gray zones is compared with that enclosed by the original illuminance curve. Among the total areas enclosed by the three current combinations, whose combinations make the area difference minimization, are those desired for the dimming control to attain the suitable electricity-to-light conversion efficacy. For the current–illuminance curve of CXB1304 LED measured in this study, the suitable three current values found by the VCSR method are 259 mA (I_4), 392 mA (I_6), and 500 mA (I_7), respectively. It should be noted that the connection of LEDs is ten in parallel; hence, the obtained current values must be multiplied by 10 times.

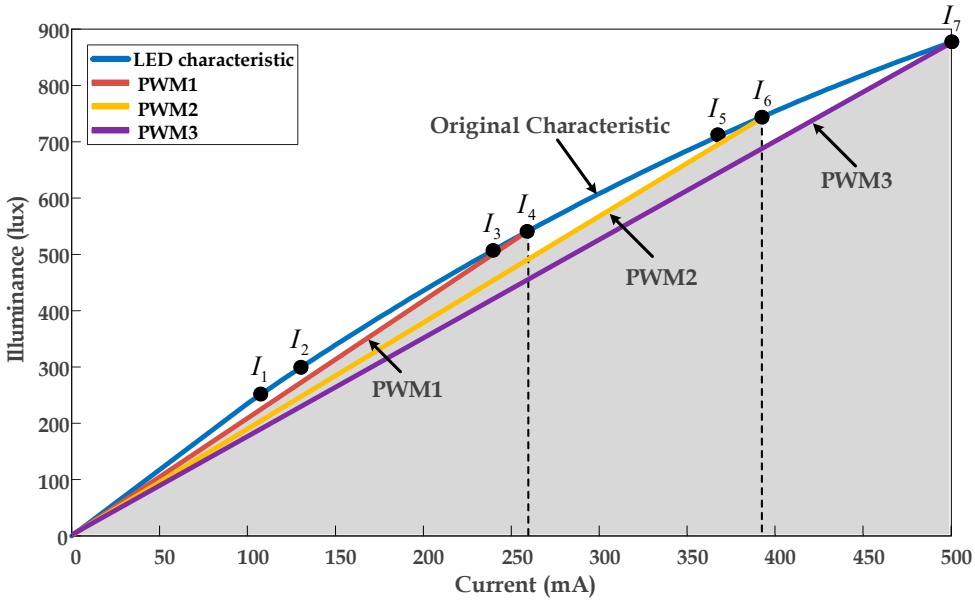

Figure 6. Illumination characteristics of the original and obtained by the other three PWM dimming controls.

For the implementation of the dimming with VCSR, two current sensing resistors are enough to satisfy the three-level current dimming control; that is, the two resistance values required can be determined via the known I_4 and I_6. However, the value of the two resistors in parallel does not promise that the LCC circuit can exactly match with controlling the LED current at the value of I_7, so three resistors with various parallel patterns are adopted here to accomplish multi-level current control. Figure 7 shows the scheme of the dimming with VCSR. In the VCSR mode, the V_r level is fixed at 1.5 V and has a 300 Hz dimming frequency. The parallel patterns of current sensing resistors (R_1, R_2 and R_3) are determined based on the dimming command through controlling the SW_{R1}, SW_{R2}, and SW_{R3} switches. To control the LED forward currents to the aforementioned values derived, the required values of R_1, R_2, and R_3 are 0.5 Ω, 1 Ω, and 1.2 Ω respectively after calculation by (11). Therefore, through the parallel pattern selection, the multilevel dimming current control can be realized and the enhancement in LED luminous efficiency is achievable as an anterior description. It should be noted that owing to the values of the three resistors used being different, up to seven levels of the current control can be attained, and the I_1, I_2, I_3, and I_5 shown in Figure 6 are the rest of the four level control current values.

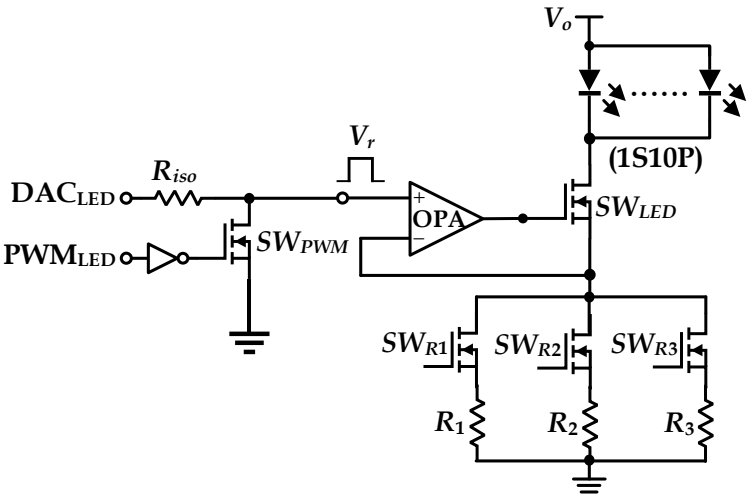

Figure 7. Scheme of the dimming with the VCSR method.

Figure 8 illustrates the control process of the dimming with VCSR. Through the different parallel combinations of three current sensing resistors, the seven-level dimming currents are generated. From small to large, they are defined as I_1 to I_7, respectively, as Figure 6 shows. The lower bound of the current in each level is the upper bound of the previous level one, and the corresponding lower limit of duty cycle of the dimming signal switch SW_{PWM} is defined as D_{dim2} to D_{dim7}, respectively. Switches SW_{R1}, SW_{R2}, and SW_{R3} are controlled by gating signals of $GPIO_{R1}$, $GPIO_{R2}$, and $GPIO_{R3}$, which are generated by the realized VCSR algorithm and are outputted through the GPIO port. The LED illumination can be dimmed by adjusting the dimming command. The larger the dimming command value, the brighter the LED, and the greater the sensed current value ADC_I. Thereby, the ADC_I can be adopted to determine whether the SW_{R1}, SW_{R2}, and SW_{R3} should be on or off to meet the dimming current control command. Hence, when the ADC_I value exceeds the upper limit of the present current level, it will be switched to the next dimming level by changing the signals of $GPIO_{R1}$, $GPIO_{R2}$, and $GPIO_{R3}$, and other than that the lower bound of the dimming duty cycle at the lowest dimming level (D_{dim0}) is zero, the initial duty cycle ($Duty_{dim}$) of the dimming signal switch SW_{PWM} is preset at the lower bound ($D_{dim(i+1)}$, i = 1~6) of the dimming duty cycle of the next level, and vice versa.

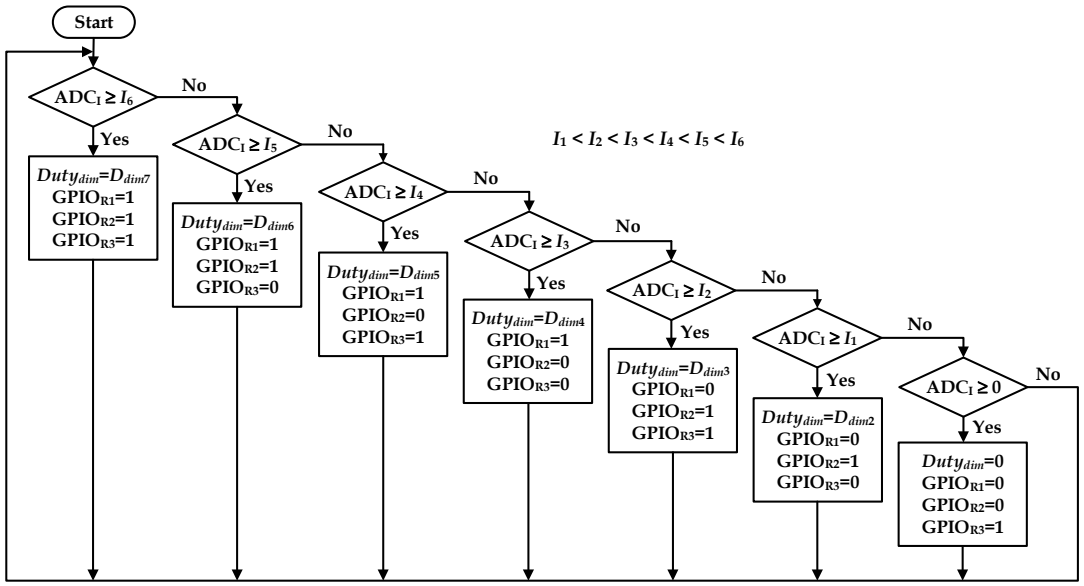

Figure 8. Control process of the dimming with VCSR.

3.2. The Dimming with VDSV

When dimming control needs more current levels by adopting the VCSR mechanism mentioned above, the hardware complexity will be unacceptable. According to (11), as the value of the current sensing resistor is fixed, the LED forward current is proportional to the voltage level of the dimming signal V_r. Therefore, another dimming signal voltage level adjustment can be utilized for multilevel dimming control to raise the luminous efficiency. The structure of the dimming control with VDSV is shown in Figure 9. It is simpler in control than the VCSR, and it is easier to achieve multi-level current control only through the tuning of the dimming signal level and duty cycle. In the VDSV mode, the values of the three current sensing resistors (R_1, R_2, and R_3) are maintained constant and are the same as those derived in the previous dimming scheme. A parallel connection can minimize the resistance value to further reduce power losses. Due to the sensing resistance being invariable, the three switches used to determine the parallel pattern of sensing resistors can also be removed.

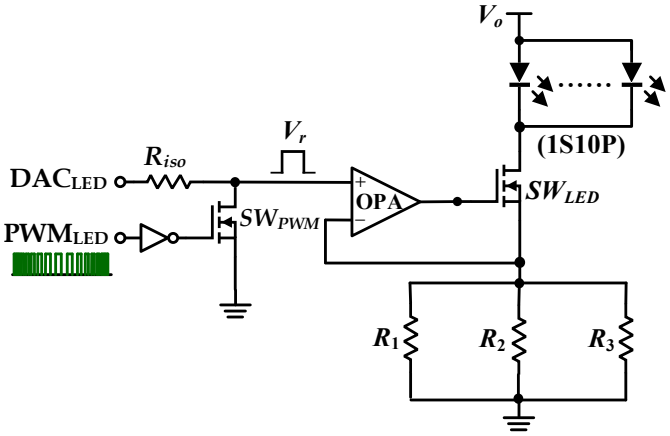

Figure 9. Scheme of the dimming with VDSV method.

According to the duty cycle figured out by the dimming PID_{dim} compensator, the gating control signal (PWM_{LED}) of SW_{PWM} is produced by the PWM_{dim} module within the DSC, which controls the SW_{PWM} to convert the variable level analog signal DAC_{LED} into the specified dimming control signal V_r to generate the target LED current. The analog level (DAC_{LED}) is obtained through the DAC conversion. This is varied based on the dimming command specified by the setting of a dimmer controller to regulate the LED forward current to the same seven levels as the VCSR scheme. Considering the tolerance of the sensing resistor value utilized, the derived seven voltage levels are 0.33 V, 0.39 V, 0.72 V, 0.78 V, 1.1 V, 1.2 V, and 1.5 V respectively. The dimmer manipulator sends these voltage signals in turn to obtain the corresponding LED dimming currents for efficiently boosting the luminous efficacy. Figure 10 illustrates the control process of the dimming with VDSV. When the ADC_I value exceeds the upper limit of the present current level, it will be switched to the next dimming level by changing the voltage level (V_{r_1}~V_{r_7}) of dimming signal V_r, and other than that the lower bound of the dimming duty cycle at the lowest dimming level (D_{dim0}) is zero, the initial duty cycle ($Duty_{dim}$) of the dimming signal switch SW_{PWM} is also preset at the lower bound ($D_{dim(i+1)}$, i = 1~6) of the dimming duty cycle of the next level, and vice versa.

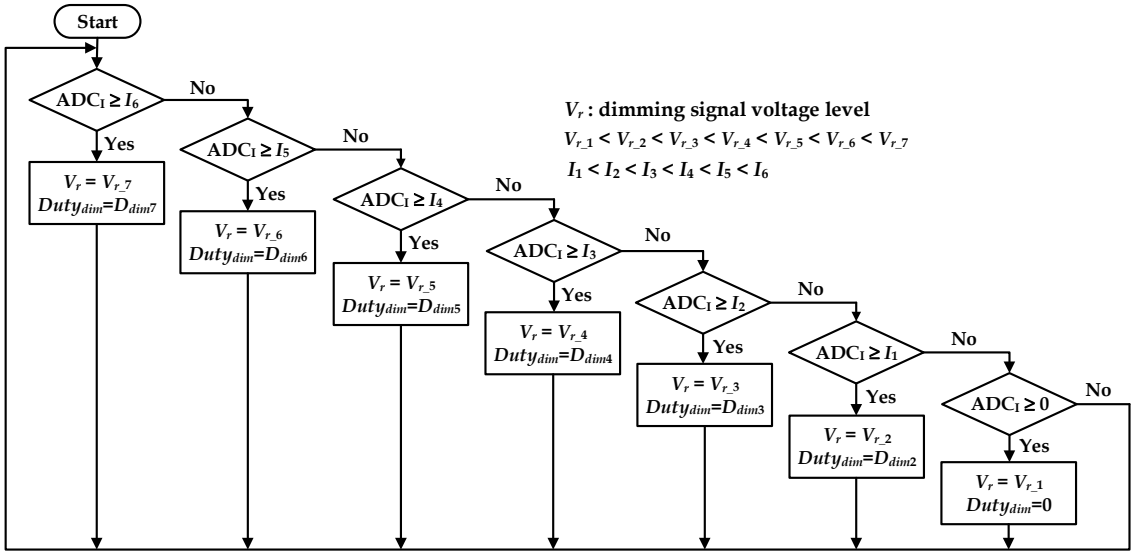

Figure 10. Control process of the dimming with VDSV.

4. Experimental Results

To verify the luminous efficiency improvement effect of the dimming methods proposed in this paper, an experimental environment for measuring precise luminosity is set up in this paper. In order to prevent other light sources in the environment from interfering with the accuracy of the illuminance measurement, a wooden box with a length, width, and height of 55 cm, 35 cm, and 30 cm was made and served as a test space. A square hole was cut on the side to facilitate wiring, which was sealed with black tape during the measuring process to decrease the measured error. The type of TES-1339R with RS-232 interface serves as the illuminometer. A photograph of the photometric environment, as shown in Figure 11, illustrates the placement of the illuminance meter, the buck converter with the dimmer and voltage controller, and the LED module mounted on the heat sink.

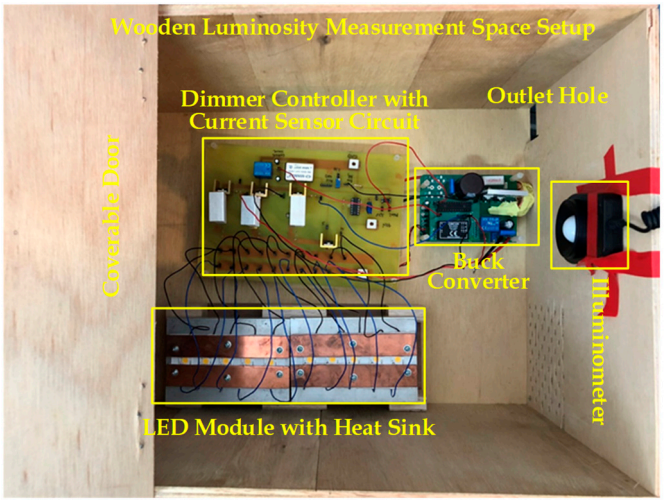

Figure 11. Photograph of the photometric environment.

This study is aimed at improving the electricity-to-light conversion efficacy of LEDs further; thereby, the illuminance versus power (I-P) curves are measured first to verify the proposed dimming methods. Figure 12a,b show the I-P curves measured with the VCSR and VDSV, respectively. The quantity on the vertical axis is the normalized illuminance, and the horizontal axis corresponds to the output power of the LED driver. The legends used in the curves represent the connection pattern among the three sensing resistors and the dimming signal voltage levels, where R_1, R_2, and R_3 are 0.5 Ω, 1 Ω, and 1.2 Ω respectively. In the VCSR dimming mode, the dimming signal voltage level V_r is maintained at 1.5 V and the resistor parallel pattern is changed to achieve the dimming control. In the VDSV dimming manner, the current-sensing resistor is kept at constant and is equal to the values of R_1, R_2, and R_3 in parallel, yet the V_r is tuned to 0.33 V, 0.39 V, 0.72 V, 0.78 V, 1.1 V, 1.2 V, and 1.5 V, respectively, to dim the LED current. From Figure 12, for the I-P curves measured with the proposed dimming methods, the illuminance envelope can be obtained by connecting the seven maximum illuminance values acquired in each dimming level. As described above in Figure 6, it can be observed from Figure 12 that the area enclosed by the illuminance envelope has been obviously approximate to that enclosed by the original LED illuminance characteristic curve, which proves that the proposed methods are significantly effective in improving the luminous efficiency.

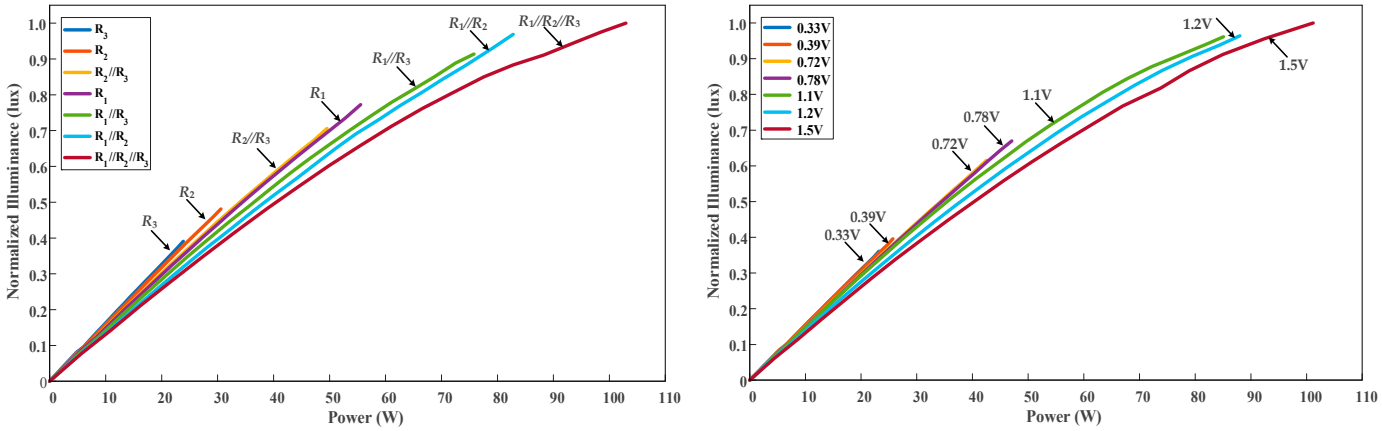

(**a**) (**b**)

Figure 12. Measured I-P curves dimmed with: (**a**) VCSR method; (**b**) VDSV method.

The quantitative computation and analysis are given to further confirm that the I-P curves measured by the studied dimming methods indeed improve the LED luminous efficiency. Comparing the proposed methods with the conventional PWM dimming, Figure 13 illustrates a conceptual diagram used to describe the estimation manner for improvement quantities of the luminous efficiency and power consumption obtained by the two dimming methods studied in this paper. When the power reaches the upper limit of the present dimming level, it will be switched to the next one. The control range of the next dimming level is from the upper bound of the previous level (i.e., the lower bound of the present level) to the upper bound of the present level, and so on. From Figure 13, under the same illuminance, the power difference between point A and point B, divided by the power value of point B, is defined as the percentage reduction of the driver power. On the other hand, as the driver output power is the same, the illuminance difference between point C and point D divided by the illuminance value of point D signifies the percentage increase of illuminance. Based on the ameliorative calculation mode as defined above, Tables 2 and 3 respectively list the quantified improvement effect of each dimming level done by the two methods, put forward as comparing with the counterpart, and Table 4 shows the entire average amelioration obtained for the full control range. From the test results, we can observe that the proposed methods have better luminous efficiencies and energy-saving effects than the conventional ones, especially as the LED is dimmed at low luminosity. This is consistent with the theoretical derivation and is closer to the actual luminous characteristics of the LED. These measured data also demonstrate the feasibility and effectiveness of the proposed methods and the remarkable advances in drive performance improvement as compared with their counterparts. Figure 14 shows the luminous efficiency (LE) curves and the corresponding LED currents of the proposed two methods and conventional PWM dimming. The entire dimming control range is divided into nine segments with a step of 10% dimming duty cycle, and the current flowing through the LED, as well as the corresponding LE obtained by three methods at each segment, are measured under the condition of feeding the identical power to light the LED. It can be seen clearly from Figure 14 that, in the low LED dimming ranges (below 80% duty cycle), the LEs of the proposed methods are better than those of the PWM dimming. From the relationship between the LED current and the LE shown in Figure 14, it can be further observed that the VDSV method has the best LE improvement performance and energy saving effect between the three methods. This is because at each dimming duty cycle, the VDSV dimming has the greatest LE boost, while the need for a driving current is least. Based on the measured data, when compared with the PWM dimming, the total average LE improvement of the devised VDSV and VCSR methods increased by 21.36% and 16.37%, respectively.

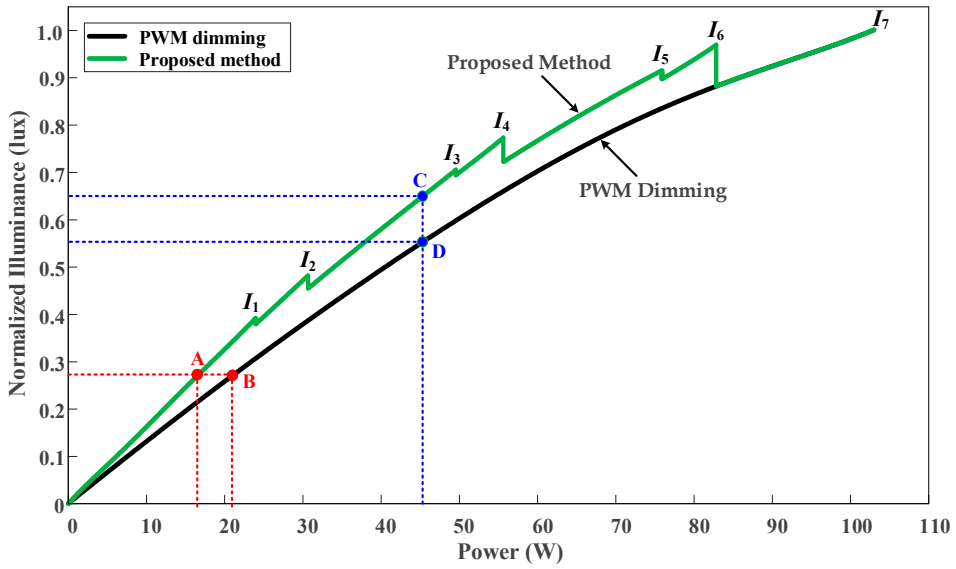

Figure 13. A conceptual diagram of the estimation method for the improvement effect.

Table 2. Quantified improvement effect of each dimming level obtained by the VCSR Method.

Item \ Level	R_3	R_2	$R_2//R_3$	R_1	$R_1//R_3$	$R_1//R_2$
Power reduction	14.5%	16.5%	14.9%	16.7%	10.9%	6.1%
Illumination boost	17.0%	18.7%	15.6%	16.5%	9.0%	3.6%

Table 3. Quantified improvement effect of each dimming level obtained by the VDSV Method.

Item \ Level	0.33 V	0.39 V	0.72 V	0.78 V	1.1 V	1.2 V
Power reduction	20.4%	20.9%	16.6%	17.1%	12.3%	13.5%
Illumination boost	24.9%	24.0%	17.5%	16.5%	9.3%	8.5%

Table 4. Quantified improvement effect for the full dimming range.

Method \ Item	Average Power Reduction	Average Illumination Boost
VCSR	13.17%	11.17%
VDSV	17.08%	13.66%

On the other hand, in order to further verify the effectiveness of the two dimming methods proposed in this paper, an integral sphere is employed to measure the color coordinates of the LED forward current at each level. Figure 15a,b show the CIE 1931 color space diagrams measured under the dimming with VCSR and VDSV, respectively. Similarly, Figure 16a,b illustrate the CIE 1976 color space diagrams measured by the two methods. Observing these diagrams, we can see that the color can stabilize in the entire dimming range. Table 5 is the maximum distance difference among the data on the color coordinate axis. It can be seen from these chromaticity diagrams and measured data that, in the color space, the seven chromaticity points are very concentrated and very close to the white light, indicating that the proposed multilevel dimming methods can make the chroma quality of the light emitted by the LED very consistent and independent of the brightness.

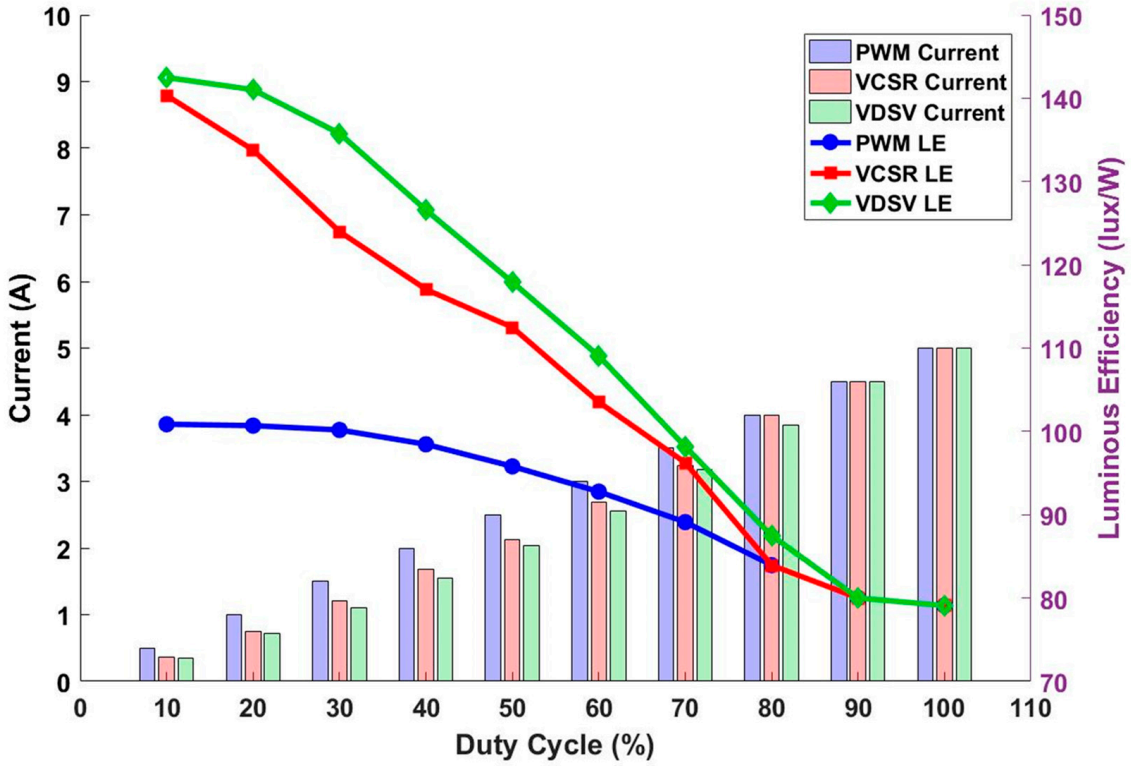

Figure 14. Luminous efficiency curves and LED current measured by the proposed methods and PWM dimming.

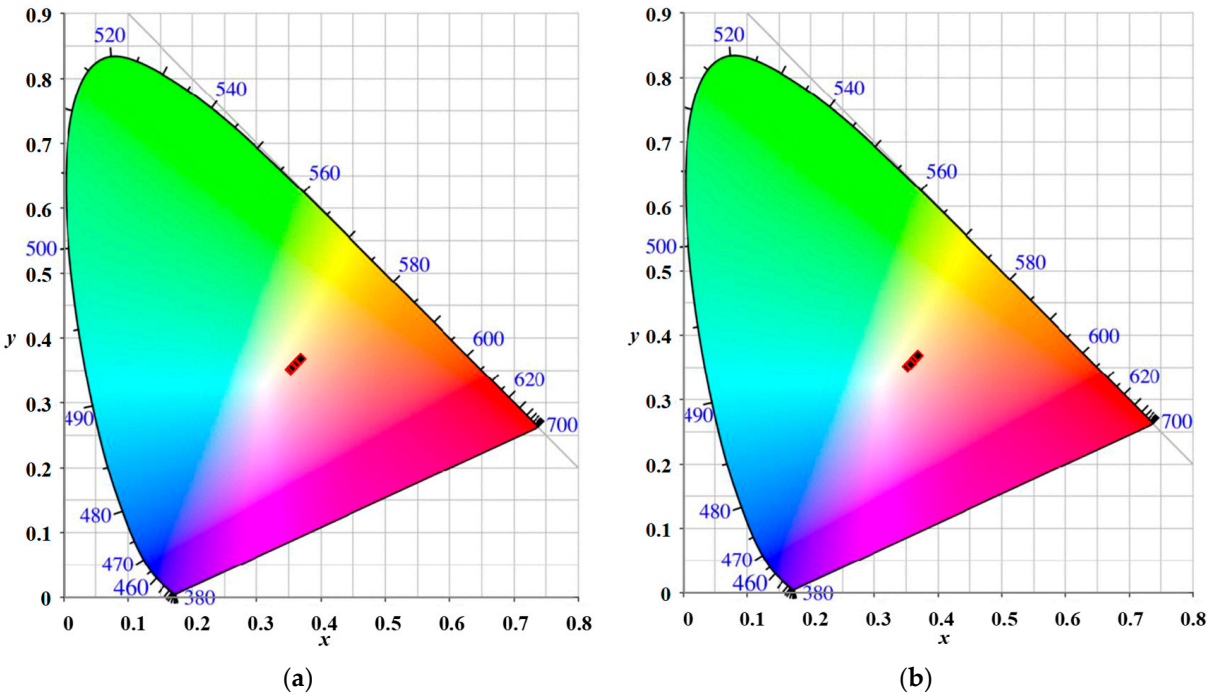

Figure 15. Measured CIE 1931 chromaticity diagrams with: (**a**) VCSR method; (**b**) VDSV method.

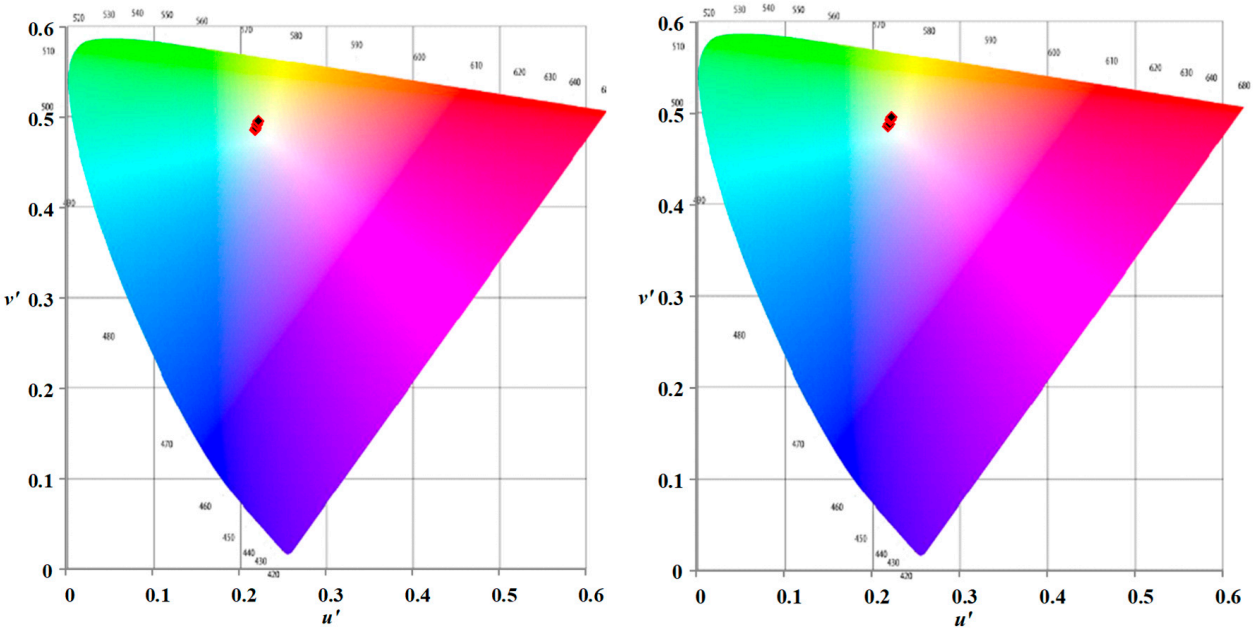

Figure 16. Measured CIE 1976 chromaticity diagrams with: (**a**) VCSR method; (**b**) VDSV method.

Table 5. Maximum change of color space coordinate axis measured with the studied methods.

Color Space / Method	CIE 1931		CIE 1976	
	Δx	Δy	$\Delta u'$	$\Delta v'$
VCSR	1.59×10^{-2}	1.68×10^{-2}	3.97×10^{-3}	1.03×10^{-2}
VDSV	1.61×10^{-2}	1.70×10^{-2}	4.04×10^{-3}	1.04×10^{-2}

5. Conclusions

Owing to the nonlinear nature of the current–illuminance characteristic curve in most LEDs, traditional PWM dimming is unable to drive the LED to exert its best luminous efficiency as specified in the datasheet under the same supplied lighting power. In this paper, we devote to the study of raising LED luminous efficacy via dimming manipulation; thus, two multilevel current dimming techniques with varied dimming signal voltages (VDSVs) and varied current sensing resistances (VCSRs) have been proposed, derived, and implemented. With limited dimming capability, the proposed dimming strategies can efficaciously enhance the luminous efficiency, meanwhile avoiding more energy consumption as compared with the PWM dimming mode. A laboratory prototype designed for a 115 W LED driver has been constructed and the proposed dimming control approaches are realized by firmware and are written into the DSC. In order to drive the LED to generate the luminosity as close to its original luminous characteristic curve as possible, the derivation of the transition value suitable for each dimming current level has been done first. Then, the experimental results are measured to validate the feasibility of the developed LED driver. Comparisons of the measured illuminance and fed power with conventional PWM dimming were also performed to evaluate the improvement effect of luminous efficacy examined in this paper.

The experimental and compared results show that, under the same illuminance generated, the average power consumption with the VDSV and VCSR methods is reduced by 17.08% and 13.17%, respectively. On the other hand, as the driver outputs the same power to light the LEDs, the generated average illuminance has an increase of 13.66% and 11.17%, respectively. In addition, the entire average LE boost has respectively increased by 21.36% and 16.37% for the full dimmable range. Accordingly, the VDSV method has the best LE improvement performance and energy saving effect among the three methods.

In the CIE1976 color space, the maximum difference between the u' coordinate measured with the two studied methods is 3.97×10^{-3} and 4.04×10^{-3}, and the maximum difference between the v' coordinates is 1.03×10^{-2} and 1.04×10^{-2}, respectively. Similarly, in the CIE1931 color space, the maximum difference between the x coordinate measured by the two studied methods is 1.59×10^{-2} and 1.61×10^{-2}, and the maximum difference between the y coordinate is 1.68×10^{-2} and 1.70×10^{-2}, respectively. The measured chromaticity diagrams and data in the color space demonstrate that the seven chromaticity points are very concentrated and are close to the white light, which also indicate that the proposed multilevel dimming method can make the chroma quality of the light emitted by the LED very consistent. Finally, the results obtained from the tests and comparisons also verify that the theoretical analysis and deduction are exactly the same and the obtained dimming curve is more in agreement with the inherent LED luminous characteristics, which also once again confirm that the devised dimming techniques indeed have the effectiveness to further enhance LED luminous efficiency and that the operation performance of multilevel dimming processes have outperformed the previous counterpart too.

Author Contributions: Conceptualization, S.-C.W. and Y.-H.L.; methodology, S.-C.W. and Y.-H.L.; software, K.-C.H.; validation, K.-C.H., S.-C.W. and Y.-H.L.; writing—original draft preparation, S.-C.W.; writing—review and editing, S.-C.W. All authors have read and agreed to the published version of the manuscript.

Funding: This research was funded by Ministry of Science and Technology, Taiwan, grant number MOST 109-2622-E-262-002-CC3.

Conflicts of Interest: The authors declare no conflict of interest.

References

1. Ponce-Silva, M.; Salazar-Pérez, D.; Rodríguez-Benítez, O.M.; Vela-Valdés, L.G.; Claudio-Sánchez, A.; De León-Aldaco, S.E.; Cortés-García, C.; Saavedra-Benítez, Y.I.; Lozoya-Ponce, R.E.; Aquí-Tapia, J.A. Flyback Converter for Solid-State Lighting Applications with Partial Energy Processing. *Electronics* **2021**, *10*, 60. [CrossRef]
2. Xu, H.; An, F.; Wen, S.; Yan, Z.; Guan, W. Three-Dimensional Indoor Visible Light Positioning with a Tilt Receiver and a High Efficient LED-ID. *Electronics* **2021**, *10*, 1265. [CrossRef]
3. Schirripa Spagnolo, G.; Leccese, F. LED Rail Signals: Full Hardware Realization of Apparatus with Independent Intensity by Temperature Changes. *Electronics* **2021**, *10*, 1291. [CrossRef]
4. Li, S.; Tan, S.; Lee, C.K.; Waffenschmidt, E.; Hui, S.Y.; Tse, C.K. A Survey, Classification, and Critical Review of Light-Emitting Diode Drivers. *IEEE Trans. Power Electron.* **2016**, *31*, 1503–1516. [CrossRef]
5. Vasilopoulou, M.; Yusoff, M.; Daboczi, M.; Conforto, J.; Gavim, A.E.; da Silva, W.J.; Macedo, A.G.; Soultati, A.; Pistolis, G.; Schneider, F.K.; et al. High Efficiency Blue Organic Light-Emitting Diodes with Below-Bandgap Electroluminescence. *Nat. Commun.* **2021**, *12*, 4868. [CrossRef] [PubMed]
6. Vasilopoulou, M.; Kim, H.P.; Kim, B.S.; Papadakis, M.; Gavim, A.E.; Macedo, A.G.; da Silva, W.J.; Schneider, F.K.; Teridi, M.A.; Coutsolelos, A.G.; et al. Efficient Colloidal Quantum Dot Light-Emitting Diodes Operating in the Second Near-infrared Biological Window. *Nat. Photon.* **2020**, *14*, 50–56. [CrossRef]
7. Yuan, F.; Zheng, X.; Johnston, A.; Wang, Y.K.; Zhou, C.; Dong, Y.; Chen, B.; Chen, H.; Fan, J.Z.; Sharma, G.; et al. Color-Pure Red Light-Emitting Diodes Based on Two-Dimensional Lead-Free Perovskites. *Sci. Adv.* **2020**, *6*, eabb0253. [CrossRef]
8. Wang, Y.K.; Yuan, F.; Dong, Y.; Li, J.Y.; Johnston, A.; Chen, B.; Saidaminov, M.I.; Zhou, C.; Zheng, X.; Hou, Y.; et al. All-Inorganic Quantum-Dot LEDs Based on a Phase-Stabilized α-$CsPbI_3$ Perovskite. *Angew. Chem. Int. Ed.* **2021**, *60*, 16164–16170. [CrossRef] [PubMed]
9. Kim, J.U.; Park, I.S.; Chan, C.-Y.; Tanaka, M.; Tsuchiya, Y.; Nakanotani, H.; Adachi, C. Nanosecond-time-scale delayed fluorescence molecule for deep-blue OLEDs with small efficiency rolloff. *Nat. Commun.* **2020**, *11*, 1–8. [CrossRef]
10. Chan, C.-Y.; Tanaka, M.; Lee, Y.-T.; Wong, Y.-W.; Nakanotani, H.; Hatakeyama, T.; Adachi, C. Stable pure-blue hyperfluorescence organic light-emitting diodes with high-efficiency and narrow emission. *Nat. Photon.* **2021**, *15*, 203–207. [CrossRef]
11. Pinti, F.; Belli, A.; Palma, L.; Gattari, M.; Pierleoni, P. Validation of Forward Voltage Method to Estimate Cracks of the Solder Joints in High Power LED. *Electronics* **2020**, *9*, 920. [CrossRef]
12. Pirc, M.; Caserman, S.; Ferk, P.; Topič, M. Compact UV LED Lamp with Low Heat Emissions for Biological Research Applications. *Electronics* **2019**, *8*, 343. [CrossRef]
13. Rachev, I.; Djamiykov, T.; Marinov, M.; Hinov, N. Improvement of the Approximation Accuracy of LED Radiation Patterns. *Electronics* **2019**, *8*, 337. [CrossRef]
14. Raggiunto, S.; Belli, A.; Palma, L.; Ceregioli, P.; Gattari, M.; Pierleoni, P. An Efficient Method for LED Light Sources Characterization. *Electronics* **2019**, *8*, 1089. [CrossRef]

15. Orem, P.M.; Vogt, K.T.; Graham, M.W.; Orem, F.M. Measuring Thermally-Driven LED Emissions via Voltage Modulation near Zero Bias. *Electronics* **2018**, *7*, 360. [CrossRef]
16. Yamada, M.; Penning, J.; Schober, S.; Lee, K.; Elliott, C. *Energy Savings Forecast of Solid-State Lighting in General Illumination Application*; U.S. Department of Energy: Washington, DC, USA, 2019.
17. Yan, Y.-H.; Cheng, H.-L.; Cheng, C.-A.; Chang, Y.-N.; Wu, Z.-X. A Novel Single-Switch Single-Stage LED Driver with Power Factor Correction and Current Balancing Capability. *Electronics* **2021**, *10*, 1340. [CrossRef]
18. Yi, K.H. High Voltage, Low Current High-Power Multichannel LEDs LLC Driver by Stacking Single-Ended Rectifiers with Balancing Capacitors. *Electronics* **2020**, *9*, 529. [CrossRef]
19. Ribas, J.; Quintana, P.J.; Cardesin, J.; Calleja, A.J.; Lopera, J.M. Closed Loop Control of a Series Class-E Voltage-Clamped Resonant Converter for LED Supply with Dimming Capability. *Electronics* **2019**, *8*, 1380. [CrossRef]
20. Liu, T.; Liu, X.; He, M.; Zhou, S.; Meng, X.; Zhou, Q. Flicker-Free Resonant LED Driver with High Power Factor and Passive Current Balancing. *IEEE Access* **2021**, *9*, 6008–6017. [CrossRef]
21. Liu, X.; Li, X.; Zhou, Q.; Xu, J. Flicker-Free Single Switch Multi-String LED Driver with High Power Factor and Current Balancing. *IEEE Trans. Power Electron.* **2019**, *34*, 6747–6759. [CrossRef]
22. Castro, I.; Vazquez, A.; Arias, M.; Lamar, D.G.; Hernando, M.M.; Sebastian, J. A Review on Flicker-free AC–DC LED Drivers for Single-Phase and Three-Phase AC Power Grids. *IEEE Trans. Power Electron.* **2019**, *34*, 10035–10057. [CrossRef]
23. Soh, M.Y.; Selvaraj, S.L.; Peng, L.; Yeo, K.S. 92.5% Average Power Efficiency Fully Integrated Floating Buck Quasi-Resonant LED Drivers Using GaN FETs. *Electronics* **2020**, *9*, 575. [CrossRef]
24. Tung, N.T.; Tuyen, N.D.; Huy, N.M.; Phong, N.H.; Cuong, N.C.; Phuong, L.M. Design and Implementation of 150 W AC/DC LED Driver with Unity Power Factor, Low THD, and Dimming Capability. *Electronics* **2019**, *9*, 52. [CrossRef]
25. Cheng, C.-A.; Chang, C.-H.; Cheng, H.-L.; Chang, E.-C.; Chung, T.-Y.; Chang, M.-T. A Single-Stage LED Streetlight Driver with Soft-Switching and Interleaved PFC Features. *Electronics* **2019**, *8*, 911. [CrossRef]
26. Ribas, J.; Quintana, P.J.; Cardesin, J.; Calleja, A.J.; Lopez-Corominas, E. Single-Switch LED Post-Regulator Based on a Modified Class-E Resonant Converter with Voltage Clamp. *Electronics* **2019**, *8*, 798. [CrossRef]
27. Garcia, J.; Saeed, S.; Quintana, P.; Cardesin, J.; Georgious, R.; Costa, M.A.D.; Camponogara, D. Optimization of a Series Converter for Low-Frequency Ripple Cancellation of an LED Driver. *Electronics* **2019**, *8*, 664. [CrossRef]
28. Tahan, M.; Hu, T. Multiple String LED Driver with Flexible and High-Performance PWM Dimming Control. *IEEE Trans. Power Electron.* **2017**, *32*, 9293–9306. [CrossRef]
29. Lv, X.; Loo, K.H.; Lai, Y.M.; Tse, C.K. Energy-Saving Driver Design for Full-Color Large-Area LED Display Panel Systems. *IEEE Trans. Ind. Electron.* **2014**, *61*, 4665–4673. [CrossRef]
30. Yang, W.H.; Yang, H.A.; Huang, C.J.; Chen, K.H.; Lin, Y.H. A High-Efficiency Single-Inductor Multiple-Output Buck-Type LED Driver with Average Current Correction Technique. *IEEE Trans. Power Electron.* **2018**, *33*, 3375–3385. [CrossRef]
31. Chen, H.; Zhou, X.; Lin, S.; Liu, J. Luminous Flux and CCT Stabilization of White LED Device with a Bi-level Driver. *IEEE Photonics J.* **2018**, *10*, 1–10.
32. Ng, S.K.; Loo, K.H.; Ip, S.K.; Lai, Y.M.; Tse, C.K.; Mok, K.T. Sequential Variable Bi-level Driving Approach Suitable for Use in High-Color-Precision LED Display Panels. *IEEE Trans. Ind. Electron.* **2012**, *59*, 4637–4645. [CrossRef]
33. Tan, S.C. General n-level Driving Approach for Improving Electrical-to-Optical Energy-Conversion Efficiency of Fast-Response Saturable Lighting Devices. *IEEE Trans. Ind. Electron.* **2010**, *57*, 1342–1353.
34. Loo, K.H.; Lia, Y.M.; Tan, S.C.; Tse, C.K. On the Color Stability of Phosphor-Converted White LEDs under dc, PWM, and Bi-level Drive. *IEEE Trans. Power Electron.* **2012**, *27*, 974–984. [CrossRef]
35. Cree Inc. XLamp LEDs. XLamp CXB1304 Datasheet 2018. Available online: https://cree-led.com/media/documents/ds-CXB1304.pdf (accessed on 21 July 2021).